

Set Twister for Single-hop Node Classification

Yangze Zhou, Vinayak Rao, Bruno Ribeiro

Purdue University
West Lafayette, IN 47906
{zhou950,varao}@purdue.edu, ribeiro@cs.purdue.edu

Abstract

Node classification is a central task in relational learning, with the current state-of-the-art hinging on two key principles: (i) predictions are permutation-invariant to the ordering of a node’s neighbors, and (ii) predictions are a function of the node’s r -hop neighborhood topology and attributes, $r \geq 2$. Both graph neural networks and collective inference methods (e.g., belief propagation) rely on information from up to r -hops away. In this work, we study if the use of more powerful permutation-invariant functions can sometimes avoid the need for classifiers to collect information beyond 1-hop. Towards this, we introduce a new architecture, the Set Twister, which generalizes DeepSets (Zaheer et al.), a simple and widely-used permutation-invariant representation. Set Twister theoretically increases expressiveness of DeepSets, allowing it to capture higher-order dependencies, while keeping its simplicity and low computational cost. Empirically, we see accuracy improvements of Set Twister over DeepSets as well as a variety of graph neural networks and collective inference schemes in several tasks, while showcasing its implementation simplicity and computational efficiency.

Introduction

In this work, we consider learning permutation-invariant representations over finite but variable-length sequences (e.g., a node’s 1-hop neighbors). This is an important inductive bias in machine learning tasks with graph-structured data, where permutation-invariance ensures that the ordering of the rows and columns of an adjacency matrix does not affect the final node representation. Deep learning architectures that ensure permutation-invariance generalize simple sum- and max-pooling operations, and allow significantly improved performance in a number of node classification tasks in relational learning. In practice, such tasks typically rely either on graph neural networks (Kipf and Welling 2017; Hamilton, Ying, and Leskovec 2017; Velickovic et al. 2018; Luan et al. 2019) or on *collective inference* (Jensen, Neville, and Gallagher 2004; Moore and Neville 2017; Sen et al. 2008) (and related methods (Huang et al. 2020)), where the labels of all nodes in a network are simultaneously predicted using a weak learner which mostly considers information only from the 1-hop neighborhood, which then is coupled with a

collective learning procedure that allows the label of a node r -hops away to influence the predictions, compensating for the weak predictive performance of the weak learners.

In this paper, we study if the use of more powerful permutation-invariant functions can eliminate the computational burden of collective inference, and allow the cost of prediction of a node to depend on its neighborhood size, rather than the network size.

A simple but powerful framework to approximate permutation-invariant functions of a sequence \mathbf{h} of neighborhood feature vectors is DeepSets (Zaheer et al. 2017). Here, each element of \mathbf{h} is independently fed into a feed-forward neural network ϕ , after which these embeddings are aggregated using a sum-pooling operation to get an intermediate permutation-invariant representation of \mathbf{h} . Finally, a nonlinear function ρ , instantiated as another neural network, is applied to get the final representation. Zaheer et al. (2017) show that with suitable choices of ϕ and ρ , any continuous permutation-invariant function over the input sequences can be approximated by the form $\rho(\sum_{j=1}^{n_{\mathbf{h}}} \phi(\mathbf{h}_j))$, where $n_{\mathbf{h}}$ denotes the length of the sequence and \mathbf{h}_j is the j th element in \mathbf{h} . Thus with universal approximators ρ and ϕ , DeepSets’s transform-sum-transform architecture itself is a universal approximator of smooth permutation-invariant functions.

The simple form of DeepSets, along with its theoretical properties (Zaheer et al. 2017; Wagstaff et al. 2019; Xu et al. 2019), have made it very attractive to practitioners. However, the learnability of the model still remains a problem if approximating the true target function requires higher-order interactions between the elements of \mathbf{h} . Examples are found when the true target function is the empirical variance or some form of minimax pairwise norm of a sequence of numbers, and complex neighborhood user feature relationship in social networks. Under the transform-sum-transform structure of DeepSets, second and higher-order interactions between elements of \mathbf{h} must be learnt by $\rho(\cdot)$ from the summed representation $\sum_{j=1}^{n_{\mathbf{h}}} \phi(\mathbf{h}_j)$. This can present a significant challenge to optimization routines and model architecture (Wagstaff et al. 2019), resulting in poor empirical performance, as noted by Murphy et al. (2019a) and confirmed by our experiments. While there has been work attempting to address this challenge (Moore and Neville 2017; Murphy et al. 2019a; Lee et al. 2019), these come at significant computational expense, making them unattractive to practitioners.

Contributions. We propose the Set Twister framework that extends DeepSets to learn richer intermediate representations, while still having comparable computational cost. Our architecture modifies the transform-sum-transform architecture of DeepSets, introducing an intermediate ‘twist’ operator that allows the representations fed into ρ to capture interactions between elements of the input sequence. We justify our approach by defining k -ary permutation-invariant interactions between elements of a sequence, and showing that our architecture is a truncation of a series expansion of such k -ary functions. In our experiments, we demonstrate how our framework offers an effective trade-off between statistical and computational performance in several tasks compared to a number of baselines from the literature. For node-classification tasks, we show how the flexibility of Set Twister can allow simpler single-hop predictions, unlike graph neural networks and collective learning schemes.

The Set Twister Architecture

We start by detailing the Set Twister architecture. We are interested in representations of permutation-invariant functions over finite but arbitrary length sequences $\mathbf{h} \in \cup_{j=1}^{\infty} \mathbb{R}^{j \times d_{\text{in}}}$. For node-classification tasks, each element of the sequence is the feature vector of a neighboring node. Write $n_{\mathbf{h}}$ for the length of the sequence \mathbf{h} , which we then write as $\mathbf{h} = (\mathbf{h}_1, \dots, \mathbf{h}_{n_{\mathbf{h}}})$, with $\mathbf{h}_i \in \mathbb{R}^{d_{\text{in}}}$.

Definition 1 (Permutation-invariant functions). *For any sequence $\mathbf{h} \in \cup_{j=1}^{\infty} \mathbb{R}^{j \times d_{\text{in}}}$ and any permutation π of the integers $(1, \dots, n_{\mathbf{h}})$, define \mathbf{h}_{π} as the reordering of the elements of \mathbf{h} according to π . A function \bar{f} is permutation-invariant if it satisfies $\bar{f}(\mathbf{h}) = \bar{f}(\mathbf{h}_{\pi})$ for all \mathbf{h} and π .*

DeepSets (Zaheer et al. 2017) defines a class of permutation-invariant functions of \mathbf{h} as

$$\text{DS}(\mathbf{h}) = \rho_{\text{DS}} \left(\sum_{j=1}^{n_{\mathbf{h}}} \phi(\mathbf{h}_j) \right). \quad (1)$$

Here ρ_{DS} and ϕ are learnable functions, typically feed-forward neural networks (MLPs). The term $\sum_{j=1}^{n_{\mathbf{h}}} \phi(\mathbf{h}_j)$ forms representations of the elements of \mathbf{h} and adds them together, thereby forming a permutation-invariant representation of the sequence \mathbf{h} . This representation is then transformed by a second function ρ_{DS} , and for powerful enough ϕ and ρ_{DS} , equation (1) can be shown to be a universal approximator of continuous permutation-invariant functions (Wagstaff et al. 2019; Zaheer et al. 2017). Despite this, Murphy et al. (2019a) shows that simply adding up representations of the elements of \mathbf{h} cannot capture dependencies between elements of the sequence, so that DeepSets effectively offloads the task of learning these high-order dependencies to $\rho_{\text{DS}}(\cdot)$. Recovering higher-order relationships from the summed representations of the individual components can be challenging, with $\rho_{\text{DS}}(\cdot)$ often failing to capture these high-order dependencies (Murphy et al. 2019a) given finite datasets. Our proposed Set Twister architecture recognizes this, and allows users to model and capture such interactions. Importantly, as we make precise later, Set Twister does this without incurring a significantly heavier computational burden than DeepSets.

Definition 2 (Set Twister architecture). *For integer-valued parameters k and M satisfying $1 \leq k \leq M$, the k -th order Set Twister representation involves M learnable permutation-invariant functions ϕ_1, \dots, ϕ_M , with $\phi_i : \mathbb{R}^{d_{\text{in}}} \rightarrow \mathbb{R}^{d_{\text{rep}}}$, $d_{\text{rep}} \geq 1$, and takes the form*

$$\begin{aligned} \text{ST}_{M,k}(\mathbf{h}) &= \rho_{\text{ST}}(\bar{f}_{M,k}(\mathbf{h})), \quad \text{where} \\ \bar{f}_{M,k}(\mathbf{h}) &= \sum_{u_1=1}^M \sum_{u_2=u_1}^M \cdots \sum_{u_k=u_{k-1}}^M \alpha_{u_1, \dots, u_k} \odot \\ &\quad \left(\sum_{i=1}^{n_{\mathbf{h}}} \phi_{u_1}(\mathbf{h}_i) \right) \odot \cdots \odot \left(\sum_{i=1}^{n_{\mathbf{h}}} \phi_{u_k}(\mathbf{h}_i) \right). \quad (2) \end{aligned}$$

Here \odot is the Hadamard product, $\rho_{\text{ST}}(\cdot)$ is a feed-forward network (MLP), and $\{\alpha_{u_1, \dots, u_k}\}_{u_1, \dots, u_k} \in \mathbb{R}^{d_{\text{rep}}}$ is a set of learnable parameter vectors. Figure 1(a) illustrates a Set Twister architecture with $M = 3$ and $k = 2$, where ϕ_i has three hidden layers, $i = 1, 2, 3$. Observe from equation (1) and Figure 1(b) that DeepSets is just a special instance of Set Twister with $M = k = 1$. In effect, Set Twister produces M intermediate representations, each in the form of DeepSets, but of smaller dimensionality (we recommend $1/M$ th the dimensionality). All size- k subsets of these M representations are then combined in a multi-linear fashion to produce the permutation-invariant representation $\bar{f}_{M,k}(\mathbf{h})$.

Set Twister for node classification: Consider a graph $G = (\mathcal{V}, A, X)$, where \mathcal{V} is the vertex set, A is the adjacency matrix, and X the node features. For any node $v \in \mathcal{V}$, write $\mathcal{N}(v)$ for the neighborhood set of node v in G , then we can construct the sequence $\mathbf{h}(v)$ as $\mathbf{h}(v) = (X_u)_{u \in \mathcal{N}(v)}$. Since the order of the neighbors does not matter, we must learn a permutation-invariant function \bar{f} on $\mathbf{h}(v)$, giving a permutation-invariant representation $\rho((\phi(X_v), \bar{f}(\mathbf{h}(v))))$ of node v . Specifically, a DeepSets representation for node v will be

$$\text{DS}^G(v) = \rho_{\text{DS}} \left((\phi(X_v), \sum_{u \in \mathcal{N}(v)} \phi(X_u)) \right), \quad (3)$$

and a Set Twister representation for node v is

$$\text{ST}_{M,k}^G(v) = \rho_{\text{ST}} \left(\phi_1(X_v), \dots, \phi_M(X_v), \bar{f}_{M,k}(\mathbf{h}(v)) \right). \quad (4)$$

Computational complexity: Let d_{rep} be the dimensionality of the permutation-invariant representation produced by Set Twister. Then, Set Twister’s forward pass—without ρ_{ST} —requires $O \left(M n_{\mathbf{h}} d_{\text{in}} d_{\text{rep}} + \binom{k+M-1}{M-1} d_{\text{rep}} \right)$ operations. The first term arises from computing the M component representations $\phi_1(\mathbf{h}_1), \phi_1(\mathbf{h}_2), \dots, \phi_M(\mathbf{h}_{n_{\mathbf{h}}})$ of the elements in the input sequence \mathbf{h} , while the second term arises from counting the number of terms in the summation in Equation (2). We note that this scales linearly in the length of \mathbf{h} : just like DeepSets, and unlike some other methods in the literature (Murphy et al. 2019a). Importantly, in the context of node classifying, $n_{\mathbf{h}}$ corresponds to the size of the neighborhood of a node, and not the size of the graph. DeepSets (without ρ_{DS}), which corresponds to Set Twister with $M = k = 1$, requires $O(n_{\mathbf{h}} d_{\text{in}} d_{\text{rep}})$ operations. In practice, to keep the number of parameters and operations comparable, a Set Twister

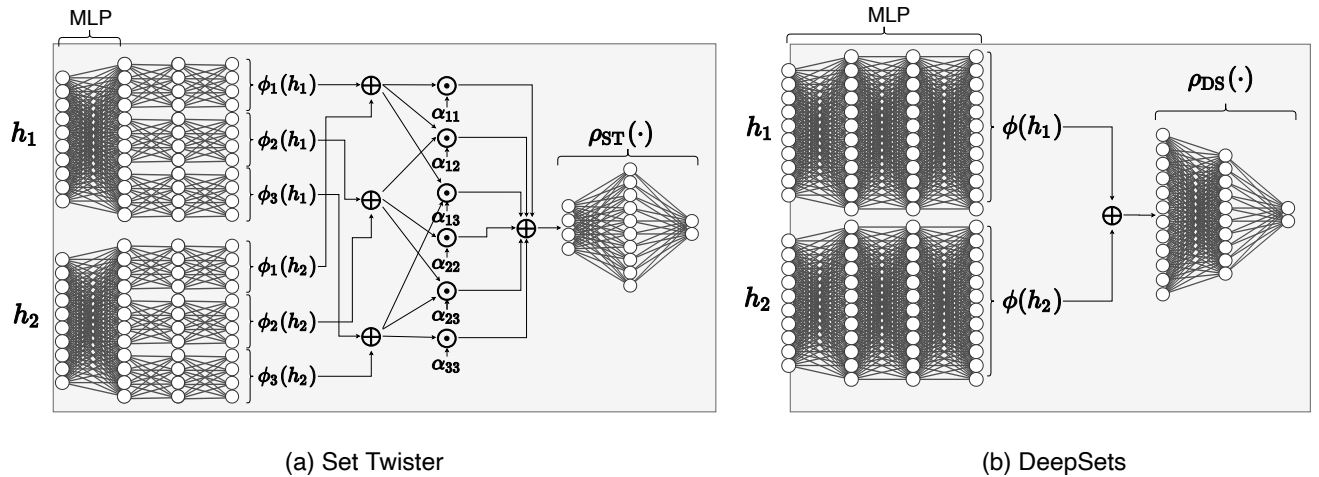


Figure 1: Illustration for input $\mathbf{h} = (\mathbf{h}_1, \mathbf{h}_2) \in \mathbb{R}^{2 \times 10}$ of (a) Set Twister architecture (with $M = 3, k = 2$ and functions $\phi_i : \mathbb{R}^{10} \rightarrow \mathbb{R}^4, i = 1, 2, 3$) v.s. (b) DeepSets architecture with same number of hidden layers and $\phi : \mathbb{R}^{10} \rightarrow \mathbb{R}^{12}$. The symbol \oplus indicates the (element-wise) sum of the vectors. Note that the illustrated Set Twister has fewer parameters than DeepSets.

architecture (when $M \geq 2$) will involve lower-dimensional representations than a comparable DeepSets architecture. Writing the dimensionality of the DeepSets representation (i.e. the output dimension of ϕ in Equation (1)) as d_{DSrep} , we recommend setting $d_{\text{rep}} = d_{\text{DSrep}}/M$, using functions $\phi_i : \mathbb{R}^{d_{\text{in}}} \rightarrow \mathbb{R}^{d_{\text{rep}}}$. With such a setting, the ϕ function of DeepSets can be viewed as a concatenation of the M functions ϕ_i of Set Twister. Our architecture modifies DeepSets by breaking the output of ϕ into M components, and following Equation (2), scrambles and recombines them. The multilinear structure of this “twisting” operation is indexed by parameters α_{u_1, \dots, u_k} .

In terms of number of parameters, the complexity for Set Twister is $O(Md_{\text{in}}d_{\text{rep}} + \binom{k+M-1}{M-1}d_{\text{rep}})$. In Figure 1, Set Twister ($M = 3, k = 2$) has 512 operations (572 if we include ρ_{ST}) and 240 learnable parameters counting all α as free parameters (300 if we include ρ_{ST}), while DeepSets has 828 operations (968 if we include ρ_{DS}) and 408 learnable parameters (548 if we include ρ_{DS}), nearly double the number of Set Twister operations and parameters. In general, limiting Set Twister to small values of M and k will keep its complexity close to, if not better than, DeepSets.

Analysis of Set Twister

In what follows, we show that without $\rho_{\text{ST}}(\cdot)$, Set Twister is provably more expressive than DeepSets. The richer representation that Set Twister learns results in reduced reliance on $\rho_{\text{ST}}(\cdot)$, allowing it to be simpler than $\rho_{\text{DS}}(\cdot)$, and making Set Twister easier to train: in most of our experiments, we find that it performs better than DeepSets. Theorem 1 presents the main theoretical result of our work, justifying the multilinear structure of Set Twister, and showing it allows us to approximate any k -ary permutation-invariant function. Theorem 2 shows that the expressive power of this class of k -ary permutation-invariant functions increases with k , by virtue of being able to capture higher-order interactions among the elements of the input sequence. All theoretical proofs will be

given in a longer version of the paper. We start by defining this class of functions.

Definition 3 (k -ary permutation-invariant functions). Consider a sequence $\mathbf{h} \in \cup_{j=1}^{\infty} \mathbb{R}^{j \times d_{\text{in}}}$, and an integer $k \in \mathbb{N}$. A k -ary permutation-invariant function $\bar{f}^{(k)}$ takes the form

$$\bar{f}^{(k)}(\mathbf{h}) = \sum_{i_1, i_2, \dots, i_k \in \{1, \dots, n_{\mathbf{h}}\}} \bar{f}^{(k)}(\mathbf{h}_{i_1}, \mathbf{h}_{i_2}, \dots, \mathbf{h}_{i_k}), \quad (5)$$

where $\bar{f}^{(k)} : \mathbb{R}^{k \times d_{\text{in}}} \rightarrow \mathbb{R}^{d_{\text{rep}}}$ is an arbitrary, possibly permutation-sensitive function. The output of the function $\bar{f}^{(k)}$ forms a k -ary representation of the input sequence \mathbf{h} .

Observe that $\bar{f}^{(k)}$ above is insensitive to reorderings of elements of \mathbf{h} , despite being composed of permutation-sensitive functions \bar{f} . Further, note that DeepSets produces a k -ary representation, with $k = 1$. A closely related definition of k -ary permutation invariance was considered in Murphy et al. (2019a), though in their implementation, computation scaled as $O(n_{\mathbf{h}}^k)$, quickly becoming impractical even for $k = 2$. The next theorem shows that despite being linear in $n_{\mathbf{h}}$, Set Twister for any k (as defined in Equation (2)) can approximate any k -ary permutation-invariant function.

Theorem 1. Under mild assumptions, the limit $\lim_{M \rightarrow \infty} \bar{F}_{M,k}(\cdot)$, with $\bar{F}_{M,k}(\cdot)$ as in Equation (2), converges in mean to Equation (5) for any $\bar{f}^{(k)}(\cdot)$ if ϕ_1, \dots, ϕ_M are universal approximators (e.g., MLPs).

The next theorem shows the significance of Definition 3, and why being able to approximate it is important: briefly, the class of k -ary functions strictly increases with k . We note once again that DeepSets, with $k = 1$, produces 1-ary representations, whereas $n_{\mathbf{h}}$ -ary representations can capture all possible permutation-invariant representations of a sequence.

Theorem 2. Assume $1 < k \leq n_{\mathbf{h}}$. Then, increasing k in Equation (5) strictly increases $\bar{f}^{(k)}$'s expressive power, that is, if \mathcal{F}_k is the set of all permutation-invariant functions of

the form $\bar{f}^{(k)}$, then \mathcal{F}_{k-1} is a proper subset of \mathcal{F}_k . Thus, a k -ary permutation-invariant function $\bar{f}^{(k)}$ can express any $(k-1)$ -ary permutation-invariant function $\bar{f}^{(k-1)}$, but the converse does not hold.

The proof of Theorem 1 hinges on Lemma 1 below, which extends a result discussed in Kreider et al. (1966, Chapter 9).

Lemma 1. Define the d_{rep} -dimensional function $\bar{f}^{(k)}$ in Definition 3 as $\bar{f}^{(k)}(\mathbf{h}_1, \dots, \mathbf{h}_k) = (\bar{f}_1^{(k)}(\mathbf{h}_1, \dots, \mathbf{h}_k), \dots, \bar{f}_{d_{rep}}^{(k)}(\mathbf{h}_1, \dots, \mathbf{h}_k))$. Assume

each component $\bar{f}_r^{(k)}$ is Riemann integrable on the domain $[a, b]^{k \times d_{in}}$ ($a, b \in \mathbb{R}$), and let $\{\gamma_u(\cdot)\}_{u=1}^\infty$ be orthogonal bases for Riemann integrable functions on $[a, b]^{d_{in}}$. Then, the set of the products $\{\gamma_{u_1}(\cdot) \cdots \gamma_{u_k}(\cdot)\}$, for $1 \leq u_1 \leq u_2 \leq \dots \leq u_k\}$ is an orthogonal basis for any Riemann integrable function on $R = [a, b]^{k \times d_{in}}$. The expansion coefficient of r -th component $\bar{f}_r^{(k)}(\cdot)$ is

$$\alpha_{u_1, \dots, u_k}^{(r)} = c_{u_1, \dots, u_k} \frac{\int \cdots \int_R \bar{f}_r^{(k)}(\mathbf{h}_1, \dots, \mathbf{h}_k) \gamma_{u_1}(\mathbf{h}_1) \cdots \gamma_{u_k}(\mathbf{h}_k) d\mathbf{h}_1 \cdots d\mathbf{h}_k}{\int \cdots \int_R \gamma_{u_1}^2(\mathbf{h}_1) \cdots \gamma_{u_k}^2(\mathbf{h}_k) d\mathbf{h}_1 \cdots d\mathbf{h}_k}, \quad (6)$$

where $c_{u_1, \dots, u_k} \in \mathbb{R}$ is a constant related to $\{u_1, \dots, u_k\}$. Thus the series expansion takes the form below (where convergence is in mean):

$$\begin{aligned} & \bar{f}_r^{(k)}(\mathbf{h}_1, \dots, \mathbf{h}_k) \\ &= \lim_{M \rightarrow \infty} \sum_{u_1=1}^M \cdots \sum_{u_k=u_{k-1}}^M \alpha_{u_1, \dots, u_k}^{(r)} \gamma_{u_1}(\mathbf{h}_1) \cdots \gamma_{u_k}(\mathbf{h}_k). \end{aligned} \quad (7)$$

Plugging the representation from Equation (7) into Equation (5), and define $\alpha_{u_1, \dots, u_k} = [\alpha_{u_1, \dots, u_k}^{(1)}, \dots, \alpha_{u_1, \dots, u_k}^{(d_{rep})}]^T$, $\tilde{\gamma}_{u_i}(\cdot) = [\gamma_{u_i}^{(1)}(\cdot), \dots, \gamma_{u_i}^{(d_{rep})}(\cdot)]^T$, we can write out a series-expansion for the entire vector-valued function $\bar{f}^{(k)}$:

$$\begin{aligned} \bar{f}^{(k)}(\mathbf{h}) &= \lim_{M \rightarrow \infty} \sum_{u_1=1}^M \cdots \sum_{u_k=u_{k-1}}^M \alpha_{u_1, \dots, u_k} \\ & \odot \left(\sum_{i=1}^{n_h} \tilde{\gamma}_{u_1}(\mathbf{h}_i) \right) \odot \cdots \odot \left(\sum_{i=1}^{n_h} \tilde{\gamma}_{u_k}(\mathbf{h}_i) \right). \end{aligned} \quad (8)$$

As before, the equations above converge in mean.

In Set Twister, we truncate the above summation for some finite M . Besides the obvious computational necessity of such a truncation, we justify this by three facts: 1) in our overall architecture, the output of the truncated sum will be passed through another neural network $\rho_{ST}(\cdot)$ which can clean up the effects of the truncation approximation (see Proposition 1 below), 2) our neural network implementation seeks to find important bases that relate to the task, and doing this in a data-driven fashion can have smaller approximation error, and 3) larger M will lead to larger model capacity, corresponding to less smooth functions. As far as the second point is concerned, it is possible to enforce orthogonality of

the components $\gamma_i(\cdot)$, though we do not do this, since this only reduces the expressiveness of our finite truncation. It is possible that enforcing orthogonality will lead to better identifiability and easier learning, however we leave investigating this for future work.

We formalize the first point below, showing that even with the finite truncation, the full Set Twister architecture is a universal approximator of any continuous permutation-invariant function for any choices of k and M .

Proposition 1. Set Twister is a universal approximator of continuous permutation-invariant functions.

Related Work

Permutation invariance Permutation invariance has been widely studied and applied in recent years, and is a basic requirement for applications involving set-valued inputs. Examples include multiple instance learning (Dietterich, Lathrop, and Lozano-Pérez 1997; Maron and Lozano-Pérez 1998), the self-attention block (encoder) of the Transformer architecture used in NLP tasks (Vaswani et al. 2017), point cloud modeling (Achlioptas et al. 2018; Qi et al. 2017), and scene understanding and image segmentation (Su et al. 2015; Kalogerakis et al. 2017; Sridhar et al. 2019).

There are several different approaches to achieve permutation-invariance in the literature. One line of work tries to find or learn a canonical orderings of input sequences related to the task at hand (Niepert, Ahmed, and Kutzkov 2016; Vinyals, Bengio, and Kudlur 2016; Zhang, Hare, and Prügel-Bennett 2019), while difficulties of such approaches have been discussed in Murphy et al. (2019a). Another popular approach is data augmentation (Cubuk et al. 2019; Fawzi et al. 2016), where the training dataset is augmented with permutations of the training sequences, thereby biasing learning towards permutation invariance.

Recent work (Lyle et al. 2020) argues that ‘‘feature averaging’’ is better than data augmentation, and justifies the most widely studied approach to permutation-invariance: by building permutation-invariance into the neural network architecture. As discussed earlier, DeepSets (Zaheer et al. 2017) uses sum-pooling over instance-based embeddings and studies its theoretical properties, while (Qi et al. 2017; Ravanbakhsh, Schneider, and Póczos 2016; Edwards and Storkey 2017) propose similar approaches using other pooling operations such as max-pooling. Wagstaff et al. (2019) studies the theoretical limits of such approaches. Murphy et al. (2019a) extends this framework to have functions with higher-order interactions. Set Transformer (Lee et al. 2019) uses self-attention blocks of a Transformer architecture to model the interaction among elements in the input. More broadly, \mathcal{G} -invariant neural networks dealing with invariance according to general group actions are discussed in (Cohen and Welling 2016; Ravanbakhsh, Schneider, and Póczos 2017; Kondor and Trivedi 2018; Bloem-Reddy and Teh 2019; Maron et al. 2018, 2019).

Graph neural networks and collective inference for node classification Graph Neural Networks (GNNs) constitute a popular class of methods for learning vertex representations (Abu-El-Haija et al. 2019; Velickovic et al. 2018; Xu et al. 2018, 2019; Murphy et al. 2019b) using neural network

to capture information up to r -hop neighborhood topology. The aggregation layer of GNNs are permutation-invariant. Truncated Krylov GCN (Luan et al. 2019) leverages multi-scale information and improves the expressive power of GCNs (Kipf and Welling 2017). GRAND (Feng et al. 2020) uses random propagation strategy to mitigate the issue of over-smoothing and non-robustness. However, the success of GNN is yet to be studied.

Collective inference (Jensen, Neville, and Gallagher 2004; Moore and Neville 2017; Sen et al. 2008) is popular in relational learning which incorporates dependencies among node labels and propagate inferences during training to strengthen poorly-expressive relational node classifiers. Hang, Neville, and Ribeiro (2021) propose a general procedure *collective learning* on GNNs to improve their expressive power. A related work Huang et al. (2020) combines shallow models that ignore the graph structure with simple post-processing procedures to exploit correlation in the label structure, and exceed or match state-of-the-art GNNs. In the paper, we also want to see if more expressive 1-hop representation is enough for existing node classification tasks.

Series decomposition Our approach of truncating an infinite series representation follows a long tradition in statistics, engineering and machine learning, starting from Principle Component Analysis (PCA) (Hotelling 1933), through Fourier series decomposition to more general orthogonal polynomials (Lyusternik and Yanpol’Ski 1965). Popular applications of such ideas for function decomposition include kernel methods and Gaussian processes (e.g. Williams and Seeger (2001)). Kipf and Welling (2017) use Chebyshev polynomial expansions to approximate graph convolutional networks in the context of of classifying nodes of graph.

Experimental results

We empirically evaluate the performance of Set Twister on a variety of tasks, in terms of prediction accuracy, mean absolute error (MAE) and computational complexity. We focus on $M = k = 2$ for Set Twister, which is one level of expressiveness above DeepSets, and has comparable compute-time to DeepSets. We first apply Set Twister on a variety of synthetic datasets to empirically show our theoretical claims. Then, we apply Set Twister on node classification tasks on well-known graph datasets, and compare with multiple graph neural networks and collective inference methods.

Synthetic tasks to validate theoretical claims

In this subsection, we consider tasks for which we know the task’s high-order dependencies. We compare Set Twister’s performance against other widely used permutation-invariant methods: DeepSets (Zaheer et al. 2017), 2-ary Janossy Pooling (Murphy et al. 2019a), Full Janossy Pooling using GRUs with attention mechanisms (JP Full) (Meng et al. 2019) and Set Transformer without inducing points (Lee et al. 2019). We consider Full JP to be the current state-of-the-art if the required compute time and the randomness of its representations are not practical issues for the task.

Arithmetic tasks: End-to-end learning over images We consider three permutation-invariant arithmetic tasks on integer sequences: Computing the empirical *variance* and *range* (from Murphy et al. (2019a)), and a new task, the *maxmin* task. The inputs are sequences of 28×28 images from InfiMNIST (Loosli, Canu, and Bottou 2007), an “infinite” dataset containing images of digits 0-9, obtained using pseudo-random deformations and translations of MNIST.

Consider a sequence \mathbf{h} consisting of $n_{\mathbf{h}}$ images of digits from the InfiMNIST dataset. Denote by \mathbf{y}_i the label of the i -th image \mathbf{h}_i in the sequence. The *variance* task receives a sequence \mathbf{h} of 5 images drawn uniformly with replacement from the dataset and predicts the variance of the image labels $\frac{1}{2n_{\mathbf{h}}^2} \sum_{i,j} (\mathbf{y}_i - \mathbf{y}_j)^2$; the *range* task receives a sequence \mathbf{h} of 5 images distributed the same way and tries to predict their range (the difference between the maximum and minimum labels). The *maxmin* task accepts a sequence of the same distribution and predicts $\max_i \min_j |\mathbf{y}_i - \mathbf{y}_j|$. The *variance* task involves learning 2-ary dependencies, while the *range* and *maxmin* tasks depend on the entire sequence (i.e., they are $n_{\mathbf{h}}$ -ary tasks). Both *variance* and *range* tasks have linear time $O(n_{\mathbf{h}})$ solutions, while computing *maxmin* scales quadratically with the sequence length.

We randomly generate 100,000 training sequences, 10,000 validation sequences and 10,000 test sequences from the InfiMNIST data for each run. We train our models in an end-to-end manner, treating the images as 784-dimensional vector inputs. We summarize the model architecture here. ϕ is set to be a MLP with 3 hidden layers, and ρ is set to be a MLP with 1 hidden layer and a scalar output. The Janossy Pooling model implementation follows Meng et al. (2019). For Set Transformer, the hidden dimension is set to be 128, and number of attention heads is 4. We optimize all the models using Adam with minibatch size 128 and learning rate 1×10^{-4} for 2,000 epochs, with the exception of Set Transformer and Full Janossy Pooling, where a learning rate of 5×10^{-4} gives better results.

For the integer-valued *range* and *maxmin* tasks, following Murphy et al. (2019a), we round the model outputs and report the test accuracy (i.e. the fraction of test data points whose output is correctly predicted). For the *variance* task, we report the test MAE. We also include running times per epoch in Table 1. To make the comparison clearer and fairer, we divide algorithms in terms of their computational cost, with MC denoting a Monte Carlo approximation.

From Table 1, we can see that Set Twister is among the best methods in the *range* and *maxmin* tasks, and in the *variance* task is second only to Full Janossy Pooling (and even in the last case, there is a significant gap between these two methods and all others). DeepSets obtained the highest accuracy in the *range* task, but struggled considerably for the variance test, where the 2-ary structure of Set Twister allowed it to easily learn the task. We emphasize that though we consider Set Twister with $k = 2$, our method performs well on the $n_{\mathbf{h}}$ -ary *range* and *maxmin* tasks. This is due to the nonlinear neural network ρ at the output (see also Proposition 1). DeepSets also includes such a neural network, however other than the *range* task, its performance is worse. This demonstrates our

Table 1: Test MAE in the variance task and test accuracy in the range & maxmin task, using image inputs. Per-epoch training times are included. MC indicates a Monte Carlo approximation. Standard deviations computed over 5 random initializations are shown in parentheses. Best results (with statistical significance determined by a two-sample t -test at $p = 0.05$) are in bold.

Cost	Model	variance		range		maxmin	
		MAE ↓	time (s/epoch)	acc. ↑	time (s/epoch)	acc. ↑	time (s/epoch)
$O(n_h)$	Set Twister ($M=k=2$)	0.200(0.007)	2.386(0.020)	0.931(0.002)	2.441(0.036)	0.931(0.003)	2.428(0.049)
	DeepSets	0.343(0.012)	1.804(0.015)	0.940(0.001)	1.842(0.012)	0.912(0.003)	1.839(0.012)
$O(n_h^2)$	JP 2-ary	0.803(0.016)	1.865(0.011)	0.885(0.004)	1.836(0.019)	0.752(0.008)	1.852(0.011)
	Set Transformer	0.327(0.020)	6.395(0.037)	0.917(0.002)	6.526(0.036)	0.825(0.010)	6.607(0.029)
MC	JP Full (GRU)	0.176(0.006)	3.993(0.021)	0.932(0.002)	4.077(0.087)	0.838(0.020)	4.085(0.041)

point that despite being a universal approximator, DeepSets can struggle with practical learning tasks. By incorporating higher-order representations, Set Twister requires a simpler $\rho(\cdot)$, and results in easier learnability, and significantly improved performance. In terms of runtime, Set Twister is about twice as fast as Set Transformer (the most expensive model) and JP Full, and comparable to DeepSets.

Arithmetic tasks over larger vocabulary sizes Our next experiment is more challenging, increasing the vocabulary size for our previous tasks from $0 - 9$ to $0 - 99$. For the *variance* and *maxmin* tasks, we input a sequence \mathbf{x} of 10 integers drawn uniformly with replacement from $\{0, 1, \dots, 99\}$, and for the *range* task, a sequence of 5 integers distributed the same way. In all tasks, rather than working with images of the digits, we now assign each number of random 100-dimensional embedding. As before, we randomly generate 100,000 training sequences, 10,000 validation sequences and 10,000 test sequences for each run.

The model architecture is similar to the previous setting thus omitted. We optimize all models using Adam with learning rate 5×10^{-4} for 2,000 epochs and minibatch size 128 for the *range* and *variance* tasks. For the *maxmin* task, we run all the models except Set Transformer and Full Janossy Pooling for 40,000 epochs using SGD with momentum, while Adam is used for Set Transformer and Full Janossy Pooling. We also use a learning rate scheduler. As before, we report test accuracy of the *range* task and test MAE of the *variance* task in Table 2, along with run times per epoch in Table 2.

For the *variance* task involving 2-ary dependencies, Set Twister, Set Transformer, and JP full perform best. DeepSets performs significantly worse in this case, struggling to capture the 2-ary interactions between the elements. Importantly, Set Twister is only slightly slower than DeepSets, and considerably faster than JP Full and Set Transformer. While Set Twister can be viewed as an approximation to JP 2-ary, it outperforms it significantly, in part due to difficulty training that model. For the n_h -ary *range* task, all models perform relatively well.

For the *maxmin* task, JP Full performs best, followed by Set Twister. All other models lag significantly behind these two, with Set Transformer performing worst. JP Full’s performance now is in contrast to its poor performance on the same task with the real image data, in part due to the availability of longer sequences: Set Twister’s performance is relatively insensitive to this setting. In additional results that are not presented, Set Twister is also relatively robust to settings of M , both in terms of predictive accuracy as well as run time,

which means in the simplest case $M = 2$ is enough to capture the dependencies in these tasks.

Node classification tasks

In this section, we apply our methods on six graph datasets (Table 4) for single-hop node classification using permutation-invariant representation, and compare against state-of-the-art (SOTA) graph neural networks and collective inference methods. The Friendster dataset is a social network graph (Teixeira, Jalaian, and Ribeiro 2019); the Pubmed, Cora and Cite-seer are three classic citation network benchmarks (Namata et al. 2012); the Arxiv is from the Open Graph Benchmark (OGB) (Hu et al. 2020); and wikiCS is a web graph (Mernyei and Cangea 2020).

Data splits. The training/validation/test split for Friendster dataset follows Teixeira, Jalaian, and Ribeiro (2019), and all the splits for other datasets are the same as Huang et al. (2020). Specifically, for wikiCS, there are 20 different training/validation splits and the test performances are averaged over these splits.

Comparison models. For permutation-invariant representations, using the input features as the raw node features, we apply DeepSets and Set Twister (reporting best results with *sum* or *mean* aggregation). For each node, we consider the neighborhood features as a sequence, obtain the permutation-invariant representation of the sequence and concatenate with the node feature itself to get node representations (as shown in Equations (3) and (4)). We do not implement Janossy Pooling due to memory issues. Set Transformer is not designed for variable-size sequence, and we use an attention-based GNN graph attention network (Velickovic et al. 2018) (GAT) for comparison. Other GNN models include graph convolutional network (Kipf and Welling 2017) (GCN), truncated Krylov GCN (Luan et al. 2019) (TK-GCN), and GRAND (Feng et al. 2020) which achieve good performance on several semi-supervised node classification tasks. We also compare with a recent collective inference method (Hang, Neville, and Ribeiro 2021), which can be applied on any GNN methods to improve the expressive power, here we use TK-GCN as a base GNN model (TK-GCN+CL). Since we have the same data splits as Huang et al. (2020), we present the best reported accuracy from their C&S model, and SOTA results from other models reported in Huang et al. (2020) as baselines.

Implementation details. The number of hidden layers was chosen between $\{2, 3\}$. The number of neurons in the hidden layers was chosen between $\{16, 32\}$ for GAT (with 8

Table 2: Test accuracy and per-epoch training times in range and maxmin tasks and test MAE in the variance task over randomly encoded inputs. MC indicates a Monte Carlo approximation. Standard deviations computed over 5 random initialization runs are shown in parentheses. Best results (with statistical significance determined by a two-sample t -test at $p = 0.05$) are in bold.

Cost	Model	variance		range		maxmin	
		MAE ↓	time (s/epoch)	acc. ↑	time (s/epoch)	acc. ↑	time (s/epoch)
$O(n_h)$	Set Twister ($M=k=2$)	0.333(0.008)	2.072(0.011)	0.944(0.004)	2.105(0.018)	0.705(0.011)	1.746(0.017)
	DeepSets	0.417(0.015)	1.501(0.016)	0.943(0.004)	1.504(0.006)	0.615(0.009)	1.246(0.003)
$O(n_h^2)$	JP 2-ary	1.276(0.079)	1.566(0.018)	0.936(0.016)	1.525(0.016)	0.612(0.015)	1.248(0.006)
	Set Transformer	0.316(0.020)	6.461(0.031)	0.999(0.001)	6.576(0.02)	0.587(0.017)	6.636(0.007)
MC	JP Full (GRU)	0.355(0.041)	4.040(0.055)	0.999(0.000)	3.742(0.072)	0.784(0.031)	4.356(0.032)

Table 3: Test accuracy (in %) for set representation model comparing with other GNN and collective inference models on six relational data. Standard deviations computed over 5 random initializations are shown in parentheses. Best results are in bold.

Model	Friendster	PubMed	Cora	Citeseer	Arxiv	wikiCS
GCN	34.19(00.49)	86.82(00.27)	88.39(00.95)	76.78(01.73)	54.15(00.43)	76.53(00.71)
GAT	32.28(00.74)	86.54(00.36)	87.95(00.55)	76.75(00.72)	54.65(00.32)	77.65(00.11)
TK-GCN	33.79(00.38)	86.01(00.18)	87.76(00.82)	76.09(00.61)	63.47(01.24)	78.77(00.50)
TK-GCN+CL	32.75(00.68)	86.12(00.14)	88.13(00.36)	77.23(00.63)	63.27(01.28)	78.83(00.43)
GRAND	34.48(00.94)	86.29(00.57)	87.95(00.75)	75.97(01.18)	63.39(00.84)	77.03(00.59)
DeepSets	34.48(00.94)	89.85(00.37)	87.06(00.68)	74.20(01.76)	66.12(00.13)	77.90(00.59)
Set Twister ($M=k=2$)	37.34(01.17)	90.15(00.29)	82.74(00.34)	71.43(02.09)	64.75(00.13)	76.58(00.77)
C&S (Huang et al. 2020)	—	89.74	89.05	76.22	70.60	82.54
SOTA	—	90.30	88.49	77.99	73.65	82.56

Table 4: Summary statistics of graph datasets.

Datasets	Classes	Nodes	Edges
Friendster	4	43,880	145,407
Pubmed	3	19,717	44,338
Cora	7	2,708	5,429
Citeseer	6	3,327	4,732
Arxiv	40	169,343	1,166,243
wikiCS	10	11,701	216,123

attention heads) and $\{128, 256, 512\}$ for all other models. For all models we used Dropout with probability 0.5. We optimized all models using Adam with learning rate chosen from $\{1 \times 10^{-3}, 5 \times 10^{-3}, 1 \times 10^{-2}\}$ and strength of weight decay was set as 5×10^{-4} . We trained all models in a full-batch end-to-end manner except C&S and SOTA reported from Huang et al. (2020). Our results show the test accuracy from the model achieving best validation accuracy.

Results. The test accuracy results are reported in Table 3. Note that the last two rows are reported results from Huang et al. (2020), thus do not have standard deviations. All the other models are trained in an end-to-end manner. Because of the highly imbalanced label distribution in the Friendster dataset, we reweight the test accuracy by the label proportion as in Teixeira, Jalaian, and Ribeiro (2019). We see that for the Friendster and PubMed datasets, single-hop node classification using Set Twister achieves the best results, while in Cora and Citeseer, Set Twister performs the worst. One reason for this is that as seen in Table 4, the Cora and Citeseer graphs have small degrees, and, thus, there are almost no higher-order dependencies to capture in the node neighborhoods. In the Arxiv dataset, which is large and dense, with similar architectures, DeepSets and Set Twister outperform most GNN and collective inference methods. We note that for the GCN and Arxiv dataset, we obtain performance results that are worse than those reported in Hu et al. (2020), and choose instead to present our results.

A takeaway is that in graphs with reasonably large neighborhoods, by only using 1-hop neighborhood information rather than the whole graph structure (r -hop information, for $r \geq 2$) and a powerful permutation-invariant classifier, we can achieve node classification performance comparable to widely-used GNN classifiers in most tasks, and to state-of-the-art methods in some of the tasks.

Conclusion

This work introduced the Set Twister representation architecture and evaluated its performance in node classification tasks, where we show set representations of immediate neighbors (1-hop information) perform as well as widely-used GNN methods, and sometimes on par with state-of-the-art methods. We argue that this is due to the increased representational power that Set Twister affords: Set Twister extends the aggregated instance-based representation used in DeepSets (Zaheer et al. 2017) to capture higher-order dependencies in the input sequence. Set Twister’s architecture is theoretically justified by connecting it to series approximations of permutation-invariant functions. In Set Twister’s simplest form ($M = 2, k = 2$), our empirical results showed significant accuracy improvements over DeepSets in most synthetic tasks, while being nearly as fast. Set Twister was also contrasted with slower, more complex methods such as Janossy Pooling $k = 2$ and $k = n_h$ (full) and Set Transformer, where the latter two are nearly 300% to 600% slower per epoch than DeepSets, respectively. Here, Set Twister ($M = 2, k = 2$) tends to obtain comparable results (being the best method in some tasks, and among the best in others). In the near future, we expect extensions of Set Twister whose algorithmic innovations will allow practitioners to explore larger k and M values, while still maintaining computation and memory efficiency as $M = 2, k = 2$, especially in applications involving longer input sequences.

References

- Abu-El-Haija, S.; Perozzi, B.; Kapoor, A.; Alipourfard, N.; Lerman, K.; Harutyunyan, H.; Ver Steeg, G.; and Galstyan, A. 2019. MixHop: Higher-Order Graph Convolutional Architectures via Sparsified Neighborhood Mixing. In *International Conference on Machine Learning*, 21–29.
- Achlioptas, P.; Diamanti, O.; Mitliagkas, I.; and Guibas, L. 2018. Learning Representations and Generative Models for 3D Point Clouds. In *International Conference on Machine Learning*, 40–49.
- Bloem-Reddy, B.; and Teh, Y. W. 2019. Probabilistic symmetry and invariant neural networks. *arXiv preprint arXiv:1901.06082*.
- Cohen, T.; and Welling, M. 2016. Group equivariant convolutional networks. In *International conference on machine learning*, 2990–2999.
- Cubuk, E. D.; Zoph, B.; Mane, D.; Vasudevan, V.; and Le, Q. V. 2019. Autoaugment: Learning augmentation strategies from data. In *Proceedings of the IEEE conference on computer vision and pattern recognition*, 113–123.
- Dietterich, T. G.; Lathrop, R. H.; and Lozano-Pérez, T. 1997. Solving the multiple instance problem with axis-parallel rectangles. *Artificial intelligence*, 89(1-2): 31–71.
- Edwards, H.; and Storkey, A. 2017. Towards a neural statistician. In *International Conference on Learning Representations*.
- Fawzi, A.; Samulowitz, H.; Turaga, D.; and Frossard, P. 2016. Adaptive data augmentation for image classification. In *2016 IEEE International Conference on Image Processing (ICIP)*, 3688–3692. Ieee.
- Feng, W.; Zhang, J.; Dong, Y.; Han, Y.; Luan, H.; Xu, Q.; Yang, Q.; Kharlamov, E.; and Tang, J. 2020. Graph Random Neural Network for Semi-Supervised Learning on Graphs. In *NeurIPS'20*.
- Fey, M.; and Lenssen, J. E. 2019. Fast Graph Representation Learning with PyTorch Geometric. In *ICLR Workshop on Representation Learning on Graphs and Manifolds*.
- Hamilton, W.; Ying, Z.; and Leskovec, J. 2017. Inductive representation learning on large graphs. In *Advances in Neural Information Processing Systems*, 1024–1034.
- Hang, M.; Neville, J.; and Ribeiro, B. 2021. A Collective Learning Framework to Boost GNN Expressiveness for Node Classification. In Meila, M.; and Zhang, T., eds., *Proceedings of the 38th International Conference on Machine Learning*, volume 139 of *Proceedings of Machine Learning Research*, 4040–4050. PMLR.
- Hotelling, H. 1933. Analysis of a complex of statistical variables into principal components. *Journal of educational psychology*, 24(6): 417.
- Hu, W.; Fey, M.; Zitnik, M.; Dong, Y.; Ren, H.; Liu, B.; Catasta, M.; and Leskovec, J. 2020. Open Graph Benchmark: Datasets for Machine Learning on Graphs. *arXiv preprint arXiv:2005.00687*.
- Huang, Q.; He, H.; Singh, A.; Lim, S.-N.; and Benson, A. 2020. Combining Label Propagation and Simple Models out-performs Graph Neural Networks. In *International Conference on Learning Representations*.
- Jensen, D.; Neville, J.; and Gallagher, B. 2004. Why collective inference improves relational classification. In *Proceedings of the tenth ACM SIGKDD international conference on Knowledge discovery and data mining*, 593–598.
- Kalogerakis, E.; Averkiou, M.; Maji, S.; and Chaudhuri, S. 2017. 3D shape segmentation with projective convolutional networks. In *Proceedings of the IEEE Conference on Computer Vision and Pattern Recognition*, 3779–3788.
- Kipf, T.; and Welling, M. 2017. Semi-supervised classification with graph convolutional networks. In *International Conference on Learning Representations*.
- Kondor, R.; and Trivedi, S. 2018. On the Generalization of Equivariance and Convolution in Neural Networks to the Action of Compact Groups. In *International Conference on Machine Learning*, 2747–2755.
- Kreider, D. L.; Kuller, R. G.; Ostberg, D. R.; and Perkins, F. W. 1966. *An Introduction to Linear Analysis*. Addison-Wesley Publishing Company, Inc. ISBN 6000627742.
- Lee, J.; Lee, Y.; Kim, J.; Kosiorek, A.; Choi, S.; and Teh, Y. W. 2019. Set Transformer: A Framework for Attention-based Permutation-Invariant Neural Networks. In Chaudhuri, K.; and Salakhutdinov, R., eds., *Proceedings of the 36th International Conference on Machine Learning*, volume 97 of *Proceedings of Machine Learning Research*, 3744–3753. Long Beach, California, USA: PMLR.
- Loosli, G.; Canu, S.; and Bottou, L. 2007. Training invariant support vector machines using selective sampling. *Large scale kernel machines*, 2.
- Luan, S.; Zhao, M.; Chang, X.-W.; and Precup, D. 2019. Break the Ceiling: Stronger Multi-scale Deep Graph Convolutional Networks. In Wallach, H.; Larochelle, H.; Beygelzimer, A.; d'Alché-Buc, F.; Fox, E.; and Garnett, R., eds., *Advances in Neural Information Processing Systems 32*, 10943–10953. Curran Associates, Inc.
- Lyle, C.; van der Wilk, M.; Kwiatkowska, M.; Gal, Y.; and Bloem-Reddy, B. 2020. On the Benefits of Invariance in Neural Networks. *arXiv preprint arXiv:2005.00178*.
- Lyusternik, L. A.; and Yanpol'Skii, A., eds. 1965. *CHAPTER IV - ORTHOGONAL SERIES AND ORTHOGONAL SYSTEMS*. Pergamon. ISBN 978-1-4831-6688-9.
- Maron, H.; Ben-Hamu, H.; Shamir, N.; and Lipman, Y. 2018. Invariant and equivariant graph networks. *arXiv preprint arXiv:1812.09902*.
- Maron, H.; Fetaya, E.; Segol, N.; and Lipman, Y. 2019. On the Universality of Invariant Networks. *arXiv preprint arXiv:1901.09342*.
- Maron, O.; and Lozano-Pérez, T. 1998. A framework for multiple-instance learning. In *Advances in neural information processing systems*, 570–576.
- Meng, C.; Yang, J.; Ribeiro, B.; and Neville, J. 2019. HATS: A Hierarchical Sequence-Attention Framework for Inductive Set-of-Sets Embeddings. In *Proceedings of the 25th ACM SIGKDD International Conference on Knowledge Discovery & Data Mining*, 783–792.

- Mernyei, P.; and Cangea, C. 2020. Wiki-CS: A Wikipedia-Based Benchmark for Graph Neural Networks. *arXiv preprint arXiv:2007.02901*.
- Moore, J.; and Neville, J. 2017. Deep Collective Inference. In *AAAI*, 2364–2372.
- Murphy, R.; Srinivasan, B.; Rao, V.; and Ribeiro, B. 2019a. Janosy Pooling: Learning Deep Permutation-Invariant Functions for Variable-Size Inputs. In *International Conference on Learning Representations*.
- Murphy, R.; Srinivasan, B.; Rao, V.; and Ribeiro, B. 2019b. Relational Pooling for Graph Representations. In Chaudhuri, K.; and Salakhutdinov, R., eds., *Proceedings of the 36th International Conference on Machine Learning*, volume 97 of *Proceedings of Machine Learning Research*, 4663–4673. Long Beach, California, USA: PMLR.
- Namata, G.; London, B.; Getoor, L.; Huang, B.; and EDU, U. 2012. Query-driven active surveying for collective classification. In *10th International Workshop on Mining and Learning with Graphs*, volume 8, 1.
- Niepert, M.; Ahmed, M.; and Kutzkov, K. 2016. Learning convolutional neural networks for graphs. In *International conference on machine learning*, 2014–2023.
- Paszke, A.; Gross, S.; Massa, F.; Lerer, A.; Bradbury, J.; Chanan, G.; Killeen, T.; Lin, Z.; Gimelshein, N.; Antiga, L.; Desmaison, A.; Kopf, A.; Yang, E.; DeVito, Z.; Raison, M.; Tejani, A.; Chilamkurthy, S.; Steiner, B.; Fang, L.; Bai, J.; and Chintala, S. 2019. PyTorch: An Imperative Style, High-Performance Deep Learning Library. In Wallach, H.; Larochelle, H.; Beygelzimer, A.; d'Alché-Buc, F.; Fox, E.; and Garnett, R., eds., *Advances in Neural Information Processing Systems 32*, 8024–8035. Curran Associates, Inc.
- Qi, C. R.; Su, H.; Mo, K.; and Guibas, L. J. 2017. Pointnet: Deep learning on point sets for 3d classification and segmentation. In *Proceedings of the IEEE Conference on Computer Vision and Pattern Recognition*, 652–660.
- Ravanbakhsh, S.; Schneider, J.; and Póczos, B. 2016. Deep Learning with Sets and Point Clouds. In *ICLR*.
- Ravanbakhsh, S.; Schneider, J.; and Póczos, B. 2017. Equivariance through parameter-sharing. In *Proceedings of the 34th International Conference on Machine Learning-Volume 70*, 2892–2901. JMLR. org.
- Sen, P.; Namata, G.; Bilgic, M.; Getoor, L.; Galligher, B.; and Eliassi-Rad, T. 2008. Collective classification in network data. *AI magazine*, 29(3): 93–93.
- Sridhar, S.; Rempe, D.; Valentin, J.; Sofien, B.; and Guibas, L. J. 2019. Multiview Aggregation for Learning Category-Specific Shape Reconstruction. In *Advances in Neural Information Processing Systems*, 2348–2359.
- Su, H.; Maji, S.; Kalogerakis, E.; and Learned-Miller, E. 2015. Multi-view convolutional neural networks for 3d shape recognition. In *Proceedings of the IEEE international conference on computer vision*, 945–953.
- Teixeira, L.; Jalaian, B.; and Ribeiro, B. 2019. Are Graph Neural Networks Miscalibrated? In *ICML Workshop on Learning and Reasoning with Graph-Structured Representations*.
- Vaswani, A.; Shazeer, N.; Parmar, N.; Uszkoreit, J.; Jones, L.; Gomez, A. N.; Kaiser, Ł.; and Polosukhin, I. 2017. Attention is all you need. In *Advances in neural information processing systems*, 5998–6008.
- Velickovic, P.; Cucurull, G.; Casanova, A.; Romero, A.; Lio, P.; and Bengio, Y. 2018. Graph attention networks. *ICLR*.
- Vinyals, O.; Bengio, S.; and Kudlur, M. 2016. Order Matters: Sequence to Sequence for Sets. *ICLR*.
- Wagstaff, E.; Fuchs, F.; Engelcke, M.; Posner, I.; and Osborne, M. A. 2019. On the Limitations of Representing Functions on Sets. In *International Conference on Machine Learning*, 6487–6494.
- Williams, C. K.; and Seeger, M. 2001. Using the Nyström method to speed up kernel machines. In *Advances in neural information processing systems*, 682–688.
- Xu, K.; Hu, W.; Leskovec, J.; and Jegelka, S. 2019. How Powerful are Graph Neural Networks? In *International Conference on Learning Representations*.
- Xu, K.; Li, C.; Tian, Y.; Sonobe, T.; Kawarabayashi, K.-i.; and Jegelka, S. 2018. Representation Learning on Graphs with Jumping Knowledge Networks. In *ICML*.
- Zaheer, M.; Kottur, S.; Ravanbakhsh, S.; Póczos, B.; Salakhutdinov, R. R.; and Smola, A. J. 2017. Deep sets. In *Advances in neural information processing systems*, 3391–3401.
- Zhang, Y.; Hare, J.; and Prügel-Bennett, A. 2019. Learning Representations of Sets through Optimized Permutations. In *International Conference on Learning Representations*.

Supplementary Material of ‘‘Set Twister for Single-hop Node Classification’’

Proof of results

In order to prove Theorem 1, we first introduce Theorem 3, which is discussed in Kreider et al. (1966, Chapter 9).

Theorem 3 (Kreider et al. (1966)). *If $\vec{f}(x, y) : \mathbb{R}^2 \rightarrow \mathbb{R}$ is a Riemann integrable function on a rectangle $[a, b] \times [c, d]$ ($a, b, c, d \in \mathbb{R}$), and $\{f_i(x)\}$ and $\{g_j(y)\}$ are orthogonal bases for the Riemann integrable functions on $[a, b]$ and $[c, d]$, then the set of the products*

$$\{f_i(x)g_j(y)\}, \quad i = 1, 2, \dots, j = 1, 2, \dots \quad (9)$$

is a basis for any Riemann integrable function on R , where R is the rectangle $a \leq x \leq b, c \leq y \leq d$.

The generalized Fourier coefficients of any Riemann integrable function \vec{f} on R is

$$\alpha_{i,j} = \frac{\iint_R \vec{f}(x, y) f_i(x) g_j(y) dR}{\iint_R f_i^2(x) g_j^2(y) dR}. \quad (10)$$

Thus the series expansion of $\vec{f}(x, y)$ can be written as

$$\sum_{i,j=1}^{\infty} \alpha_{i,j} f_i(x) g_j(y) \quad (11)$$

This series converges in mean to $\vec{f}(x, y)$.

The proof for this theorem can be found in Kreider et al. (1966, Chapter 9). As pointed out in Kreider et al. (1966), it can be applied for functions of any finite number of variables. A following Lemma 1 is introduced in our paper, which leads to the proof of Theorem 1. Note that we did not include the following constants $c_{u_1, \dots, u_k} \in \mathbb{R}$ in Equation (6) of Lemma 1 in the main manuscript, but make them explicit below.

Lemma 1. *Define the d_{rep} -dimensional function $\vec{f}^{(k)}$ in Definition 3 as $\vec{f}^{(k)}(\mathbf{h}_1, \dots, \mathbf{h}_k) = (\vec{f}_1^{(k)}(\mathbf{h}_1, \dots, \mathbf{h}_k), \dots, \vec{f}_{d_{rep}}^{(k)}(\mathbf{h}_1, \dots, \mathbf{h}_k))$. Assume*

each component $\vec{f}_r^{(k)}$ is Riemann integrable on the domain $[a, b]^{k \times d_{in}}$ ($a, b \in \mathbb{R}$), and let $\{\gamma_u(\cdot)\}_{u=1}^{\infty}$ be orthogonal bases for Riemann integrable functions on $[a, b]^{d_{in}}$. Then, the set of the products $\{\gamma_{u_1}(\cdot) \cdots \gamma_{u_k}(\cdot)\}$, for $1 \leq u_1 \leq u_2 \leq \dots \leq u_k$ is an orthogonal basis for any Riemann integrable function on $R = [a, b]^{k \times d_{in}}$. The expansion coefficient of r -th component $\vec{f}_r^{(k)}(\cdot)$ is

$$\alpha_{u_1, \dots, u_k}^{(r)} = c_{u_1, \dots, u_k} \cdot \frac{\int \cdots \int_R \vec{f}_r^{(k)}(\mathbf{h}_1, \dots, \mathbf{h}_k) \gamma_{u_1}(\mathbf{h}_1) \cdots \gamma_{u_k}(\mathbf{h}_k) d\mathbf{h}_1 \cdots d\mathbf{h}_k}{\int \cdots \int_R \gamma_{u_1}^2(\mathbf{h}_1) \cdots \gamma_{u_k}^2(\mathbf{h}_k) d\mathbf{h}_1 \cdots d\mathbf{h}_k}, \quad (6)$$

where $c_{u_1, \dots, u_k} \in \mathbb{R}$ is a constant related to $\{u_1, \dots, u_k\}$. Thus the series expansion takes the form below (where con-

vergence is in mean):

$$\begin{aligned} & \vec{f}_r^{(k)}(\mathbf{h}_1, \dots, \mathbf{h}_k) \\ &= \lim_{M \rightarrow \infty} \sum_{u_1=1}^M \cdots \sum_{u_k=u_{k-1}}^M \alpha_{u_1, \dots, u_k}^{(r)} \gamma_{u_1}(\mathbf{h}_1) \cdots \gamma_{u_k}(\mathbf{h}_k). \end{aligned} \quad (7)$$

Proof. Theorem 3 can be extended to functions of any finite number of variables. So if $\{f_i(x)\}$ are orthogonal bases for the Riemann integrable functions on $[a, b]$, then the set of the products

$$\{f_{i_1}(x_1) f_{i_2}(x_2) \cdots f_{i_{k_{d_{in}}}}(x_{k_{d_{in}}})\}, \quad i_1, i_2, \dots, i_{k_{d_{in}}} = 1, 2, \dots \quad (12)$$

is an orthogonal basis for any Riemann integrable function on $[a, b]^{k \times d_{in}}$.

Also $\{f_{i_1}(x_1) f_{i_2}(x_2) \cdots f_{i_{d_{in}}}(x_{d_{in}})\}$, $i_1, i_2, \dots, i_{d_{in}} = 1, 2, \dots$ is an orthogonal basis for any Riemann integrable function on $[a, b]^{d_{in}}$, define it as $\gamma_u(\mathbf{h})$, $u = 1, 2, \dots$, where $\mathbf{h} = (x_1, x_2, \dots, x_{d_{in}})$. Then $\gamma_u(\mathbf{h})$, $u = 1, 2, \dots$ is an orthogonal basis for any Riemann integrable function on $[a, b]^{d_{in}}$. Thus

$$\{\gamma_{u_1}(\cdot) \cdots \gamma_{u_k}(\cdot)\}, \quad u_i = 1, 2, \dots, i = 1, \dots, k \quad (13)$$

is an orthogonal basis for any Riemann integrable function on $[a, b]^{k \times d_{in}}$. To remove repeated function bases, we can define $1 \leq u_1 \leq u_2 \leq \dots \leq u_k$, then the set of the products $\{\gamma_{u_1}(\cdot) \cdots \gamma_{u_k}(\cdot)\}$, for $1 \leq u_1 \leq u_2 \leq \dots \leq u_k$ is an orthogonal basis for any Riemann integrable function on $[a, b]^{k \times d_{in}}$.

By Theorem 3, we can calculate the corresponding generalized Fourier coefficients. Since we combine all the repeated bases in one expression, we introduce the constants c_{u_1, \dots, u_k} here to handle it. The constants c_{u_1, \dots, u_k} is related to the repeated elements in $\{u_1, \dots, u_k\}$. Although we do not give the explicit expression of c_{u_1, \dots, u_k} , it is clear there must exist such constants to satisfy the equations. \square

Theorem 1 is a direct use of Lemma 1 as shown in the paper. We give the formal proof here.

Theorem 1. *Under mild assumptions, the limit $\lim_{M \rightarrow \infty} \vec{f}_{M,k}(\cdot)$, with $\vec{f}_{M,k}(\cdot)$ as in Equation (2), converges in mean to Equation (5) for any $\vec{f}^{(k)}(\cdot)$ if ϕ_1, \dots, ϕ_M are universal approximators (e.g., MLPs).*

Proof. The mild assumptions stated here corresponds to the assumption in Lemma 1, which means each component $\vec{f}_r^{(k)}$ of $\vec{f}^{(k)}$ in Definition 3 is Riemann integrable on the domain $[a, b]^{k \times d_{in}}$ ($a, b \in \mathbb{R}$).

We use the same definition for $\{\gamma_u(\cdot)\}_{u=1}^{\infty}$ and $\alpha_{u_1, \dots, u_k}^{(r)}$ as in Lemma 1. Plugging the representation from Lemma 1 into Equation (5), it follows that the series expansion $\vec{f}_r^{(k)}(\mathbf{h})$, the r -th component of the permutation-invariant function \vec{f}

takes the form:

$$\begin{aligned}
\bar{f}_r^{(k)}(\mathbf{h}) &= \sum_{i_1, i_2, \dots, i_k \in \{1, \dots, n_h\}} \bar{f}_r^{(k)}(\mathbf{h}_{i_1}, \mathbf{h}_{i_2}, \dots, \mathbf{h}_{i_k}) \\
&= \sum_{i_1, i_2, \dots, i_k \in \{1, \dots, n_h\}} \lim_{M \rightarrow \infty} \sum_{u_1=1}^M \cdots \sum_{u_k=u_{k-1}}^M \\
&\quad \alpha_{u_1, u_2, \dots, u_k}^{(r)} \gamma_{u_1}(\mathbf{h}_{i_1}) \cdots \gamma_{u_k}(\mathbf{h}_{i_k}) \\
&= \lim_{M \rightarrow \infty} \sum_{u_1=1}^M \cdots \sum_{u_k=u_{k-1}}^M \alpha_{u_1, u_2, \dots, u_k}^{(r)} \\
&\quad \left(\sum_{i=1}^{n_h} \gamma_{u_1}(\mathbf{h}_i) \right) \cdots \left(\sum_{i=1}^{n_h} \gamma_{u_k}(\mathbf{h}_i) \right). \tag{14}
\end{aligned}$$

By defining $\alpha_{u_1, u_2, \dots, u_k} = [\alpha_{u_1, u_2, \dots, u_k}^{(1)}, \dots, \alpha_{u_1, u_2, \dots, u_k}^{(d_{\text{rep}})}]^T$, and $\tilde{\gamma}_{u_i}(\cdot) = [\gamma_{u_i}^{(1)}(\cdot), \dots, \gamma_{u_i}^{(d_{\text{rep}})}(\cdot)]^T$, we can write out a series-expansion for the entire vector-valued function $\bar{f}^{(k)}$:

$$\begin{aligned}
\bar{f}^{(k)}(\mathbf{h}) &= \lim_{M \rightarrow \infty} \sum_{u_1=1}^M \cdots \sum_{u_k=u_{k-1}}^M \alpha_{u_1, u_2, \dots, u_k} \odot \\
&\quad \left(\sum_{i=1}^{n_h} \tilde{\gamma}_{u_1}(\mathbf{h}_i) \right) \odot \cdots \odot \left(\sum_{i=1}^{n_h} \tilde{\gamma}_{u_k}(\mathbf{h}_i) \right). \tag{15}
\end{aligned}$$

As before, the equations above converge in mean.

If ϕ_i are universal approximators of $\tilde{\gamma}_i$ for $i = 1, \dots, M$, and $\alpha_{u_1, u_2, \dots, u_k}$ are learnable parameters, then $\bar{f}_{M,k}(\cdot)$ in Equation (2) is a universal approximator of $\sum_{u_1=1}^M \cdots \sum_{u_k=u_{k-1}}^M \alpha_{u_1, u_2, \dots, u_k} \odot (\sum_{i=1}^{n_h} \tilde{\gamma}_{u_1}(\mathbf{h}_i)) \odot \cdots \odot (\sum_{i=1}^{n_h} \tilde{\gamma}_{u_k}(\mathbf{h}_i))$.

Thus the limit $\lim_{M \rightarrow \infty} \bar{f}_{M,k}(\cdot)$, with $\bar{f}_{M,k}(\cdot)$ as in Equation (2), converges *in mean* to Equation (5) for any $\bar{f}^{(k)}(\cdot)$. \square

We now restate Theorem 2 and show the proof. Note that Theorem 2 is different from Theorem 2.1 in Murphy et al. (2019a) because we allow repeated elements in $\{u_1, \dots, u_k\}$ as shown in Equation (5) while they focus on all possible permutations of the input sequence.

Theorem 2. *Assume $1 < k \leq n_h$. Then, increasing k in Equation (5) strictly increases $\bar{f}^{(k)}$'s expressive power, that is, if \mathcal{F}_k is the set of all permutation-invariant functions of the form $\bar{f}^{(k)}$, then \mathcal{F}_{k-1} is a proper subset of \mathcal{F}_k . Thus, a k -ary permutation-invariant function $\bar{f}^{(k)}$ can express any $(k-1)$ -ary permutation-invariant function $\bar{f}^{(k-1)}$, but the converse does not hold.*

Proof. ($\mathcal{F}_{k-1} \subset \mathcal{F}_k$): Consider any element $\bar{f}^{(k-1)} \in \mathcal{F}$ and write $\bar{f}^{(k-1)}$ for its associated permutation sensitive function.

For any sequence \mathbf{h} , define $\downarrow_k(\mathbf{h})$ as its projection to a length k sequence; in particular, if $n_h > k$, keep the first k elements.

Then we can have $\bar{f}^{(k-1)}(\mathbf{h}_{i_1}, \dots, \mathbf{h}_{i_{(k-1)}}) = \bar{f}^{(k-1)}(\downarrow_{k-1}(\mathbf{h}_{i_1}, \dots, \mathbf{h}_{i_{(k-1)}, \mathbf{h}_{i_k}})) := n_h \bar{f}_+^{(k)}(\mathbf{h}_{i_1}, \dots, \mathbf{h}_{i_{(k-1)}, \mathbf{h}_{i_k}})$, $\forall i_1, i_2, \dots, i_k \in \{1, \dots, n_h\}$, where we define the function $\bar{f}_+^{(k)}$ over k elements but only looks at its first $k-1$ elements.

$$\begin{aligned}
\bar{f}^{(k-1)}(\mathbf{h}) &= \sum_{i_1, \dots, i_{(k-1)} \in \{1, \dots, n_h\}} \bar{f}^{(k-1)}(\mathbf{h}_{i_1}, \dots, \mathbf{h}_{i_{(k-1)}}) \\
&= \frac{1}{n_h} \sum_{i_1, \dots, i_{(k-1)}, i_k \in \{1, \dots, n_h\}} \bar{f}^{(k-1)} \\
&\quad (\downarrow_{k-1}(\mathbf{h}_{i_1}, \dots, \mathbf{h}_{i_{(k-1)}, \mathbf{h}_{i_k}})) \\
&= \sum_{i_1, \dots, i_k \in \{1, \dots, n_h\}} \bar{f}_+^{(k)}(\mathbf{h}_{i_1}, \dots, \mathbf{h}_{i_k}) = \bar{f}^{(k)}(\mathbf{h}) \tag{16}
\end{aligned}$$

where $\bar{f}^{(k)} \in \mathcal{F}_k$.

($\mathcal{F}_k \not\subset \mathcal{F}_{k-1}$) We need to find $\bar{f}^{(k)} \in \mathcal{F}_k$ such that $\bar{f}^{(k-1)} \neq \bar{f}^{(k)}$ for all $\bar{f}^{(k-1)} \in \mathcal{F}_{k-1}$. Let $\bar{f}^{(k)}$ and $\bar{f}^{(k-1)}$ be associated with $\bar{f}^{(k)}$ and $\bar{f}^{(k-1)}$, respectively.

Without loss of generality, consider $n_h = k$. Let $\bar{f}^{(k)}(\mathbf{h}) = \prod_{i=1}^{n_h} \mathbf{h}_i$, assuming all the elements \mathbf{h}_i are just scalars. So the resulting $\bar{f}^{(k)}(\mathbf{h})$ must be continuous and differentiable with respect to $\mathbf{h}_i, i = 1, \dots, k$. Thus $\frac{\partial \bar{f}^{(k)}(\mathbf{h})}{\partial \mathbf{h}_1 \partial \mathbf{h}_2 \cdots \partial \mathbf{h}_k} = k!$.

Assume there exists a function $\bar{f}^{(k-1)}(\mathbf{h}) \in \mathcal{F}_{k-1}$, such that $\bar{f}^{(k-1)} = \bar{f}^{(k)}$. Then for any \mathbf{h} , the derivative with respect to the elements should also be the same. However, since $\bar{f}^{(k-1)}$ takes at most $k-1$ distinct variables, $\frac{\partial \bar{f}^{(k-1)}(\mathbf{h})}{\partial \mathbf{h}_1 \partial \mathbf{h}_2 \cdots \partial \mathbf{h}_k} = 0$, which contradicts our assumption. So there is not such a function in \mathcal{F}_{k-1} . We conclude our proof that $\mathcal{F}_k \not\subset \mathcal{F}_{k-1}$. \square

Finally we restate Proposition 1 and show the proof.

Proposition 1. *Set Twister is a universal approximator of continuous permutation-invariant functions.*

Proof. If we set all the coefficients $\alpha_{u_1, u_2, \dots, u_k}$ to be $\vec{0} \in \mathbb{R}^{d_{\text{rep}}}$ except $\alpha_{1, 2, \dots, k} = \vec{1} \in \mathbb{R}^{d_{\text{rep}}}$, and let ϕ_2, \dots, ϕ_k all output $\vec{1} \in \mathbb{R}^{d_{\text{rep}}}$ (can be satisfied by the universal approximation ability of MLP), then the Set Twister has the exact same structure as DeepSets (Zaheer et al. 2017), which means DeepSets is included in the structure of Set Twister for any choices of k and M . The remainder of the proof follows from the proof discussed in the Appendix of Zaheer et al. (2017). Hence Set Twister is a universal approximator of continuous permutation invariant functions. \square

Table 5: Number of trainable parameters for different models using image (all tasks) and randomly encoded inputs (variance and range tasks). MC indicates a Monte Carlo approximation.

Cost	Model	Image inputs	Encoded integers
$O(n_h)$	Set Twister ($M=k=2$)	272011	6031
	DeepSets	277861	9481
$O(n_h^2)$	JP 2-ary	513061	9481
	Set Transformer	385281	40833
MC	JP Full (GRU)	433622	102122

Table 6: Number of trainable parameters for different models using randomly encoded inputs in the maxmin task with various sequence length. MC indicates a Monte Carlo approximation.

Cost	Model	$n_h = 10$	$n_h = 20$
$O(n_h)$	Set Twister ($M=k=2$)	12221	25391
	Set Twister ($M=3, k=2$)	11171	22091
	DeepSets	15371	35291
$O(n_h^2)$	JP 2-ary	15371	35291
	Set Transformer	40833	40833
MC	JP Full (GRU)	100572	100572

Implementation Details for synthetic tasks

We discussed most of our implementation details in the paper. We compare Set Twister’s performance against widely used permutation-invariant representations on a variety of tasks for which we know the task’s high-order dependencies: DeepSets (Zaheer et al. 2017), 2-ary Janossy Pooling (Murphy et al. 2019a), Full Janossy Pooling using GRUs with attention mechanisms (JP Full) (Meng et al. 2019) and Set Transformer without inducing points (Lee et al. 2019). We extended the code from Murphy et al. (2019a) for most of our tasks. We chose to use `tanh` activation over `relu` activation in most of our tasks because of better performance. For optimization, we searched over Adam and SGD with momentum (equal to 0.9), and $\{1 \times 10^{-4}, 5 \times 10^{-4}, 1 \times 10^{-3}, 5 \times 10^{-3}\}$ for learning rate to achieve better performance. For the loss function, we always used the L1 loss in our experiments. In the *maxmin* task, we used a learning rate scheduler which decrease the learning rate by a factor of 0.9 if the validation accuracy has stopped improving in the past 500 epochs. Training was performed on NVIDIA GeForce RTX 2080 Ti GPUs.

When comparing with all the other baselines, we made sure the number of parameters was comparable (see Tables 5 and 6). Since we use different neural network structures for the *maxmin* task with various sequence lengths over randomly encoded inputs, we report the number of the parameters in a separate Table 6. As we can see, Set Twister always has the smallest number of parameters. Note that although theoretically, Set Twister will have much more parameters if M and k are large. However, by setting $d_{\text{rep}} = d_{\text{DSrep}}/M$ as shown in Figure 1(a), the number of trainable parameters for Set Twister is much less than the corresponding DeepSets model when $k = 2$.

For the implementation details of Set Twister, we use a mask matrix to update only sub-elements of the weight ma-

trix as shown in Figure 1(a). For $k = 2$, instead of restricting $u_1 \leq u_2 \leq M$ as discussed in Equation (2), we allow repeated products by setting $u_1 \leq M, u_2 \leq M$ for computation simplicity. To be more specific, α_{u_1, u_2} and α_{u_2, u_1} will be considered as different learnable coefficients when $u_1 \neq u_2$. The number of coefficients will increase from $\binom{k+M-1}{M-1} d_{\text{rep}}$ to $M^k d_{\text{rep}}$. However, in the case of $k = 2$ with small M and setting $d_{\text{rep}} = d_{\text{DSrep}}/M$, it will not cause problems as shown in Tables 5 and 6. For Full Janossy Pooling, we use bidirectional GRU with attention as stated in Meng et al. (2019), and use 1 randomly chosen permutations at test time for Monte Carlo estimation.

Implementation Details for node classification tasks

All neural network approaches, including the models proposed in this paper, are implemented in PyTorch (Paszke et al. 2019) and Pytorch Geometric (Fey and Lenssen 2019).

Our GCN (Kipf and Welling 2017) and GAT (Velickovic et al. 2018) implementations are based on their Pytorch Geometric implementations. In table Table 3, the results for DeepSets and Set Twister are reported using the best performed aggregation (*sum* or *mean*) in validation. For all the other models, we use the code in github and make sure we follow the model architecture.

The number of hidden layers was chosen between $\{2, 3\}$. Specifically, the ϕ and ρ neural network in DeepSets and Set Twister can both have $\{2, 3\}$ hidden layers. The number of neurons in the hidden layers was chosen between $\{16, 32\}$ for GAT (with 8 attention heads) and $\{128, 256, 512\}$ for all other models. For all models we used Dropout with probability 0.5. We optimized all models using Adam with learning rate chosen from $\{1 \times 10^{-3}, 5 \times 10^{-3}, 1 \times 10^{-2}\}$ and strength of weight decay was set as 5×10^{-4} . We trained all models in a full-batch end-to-end manner except C&S and SOTA reported from Huang et al. (2020). Our results show the test accuracy from the model achieving best validation accuracy. Early stopping with patience 200 was also used.

For Set Twister, since we have various sized neighborhood in the graph data, the implementation is slightly different than the synthetic tasks. We will fast pass all node features into a ϕ neural network. And then, we will create a mask matrix which encodes the neighborhood nodes for each node (edge relationship) as a sparse adjacency matrix, so only the values of the edge indexes are 1. Then using this sparse adjacency matrix, we can do a matrix multiplication with the obtained ϕ representation for all the nodes, we get a summed (or mean) representation from the neighborhood nodes for all nodes. Finally, we concatenate the aggregated feature in the neighborhood and the original node representation, and feed into another ρ neural network.

More experimental results

The ability of Set Twister to learn 2-ary dependencies

Following Murphy et al. (2019a), we explore setting the upper layer ρ to be a linear layer: a feed-forward layer with identity

Table 7: Test accuracy and per-epoch training time in the maxmin task under different sequence lengths. Standard deviations computed over 5 runs are shown in parentheses. Best results (with significance determined by a two-sample t -test at $p = 0.05$) are in bold.

Cost	Model	$n_h=10$		$n_h=20$	
		acc.↑	time (s/epoch)	acc.↑	time (s/epoch)
$O(n_h)$	Set Twister ($M=k=2$)	0.705(0.011)	1.746(0.017)	0.616(0.027)	1.768(0.015)
	Set Twister ($M=3, k=2$)	0.702(0.007)	1.751(0.010)	0.632(0.012)	1.748(0.015)
	DeepSets	0.615(0.009)	1.246(0.003)	0.538(0.012)	1.251(0.005)
$O(n_h^2)$	JP 2-ary	0.612(0.015)	1.248(0.006)	0.438(0.014)	1.248(0.009)
	Set Transformer	0.587(0.017)	6.636(0.007)	0.392(0.012)	6.602(0.034)
MC	JP Full (GRU)	0.784(0.031)	4.356(0.032)	0.868(0.018)	4.829(0.040)

Table 9: Test accuracy and per-epoch training times in range task and test MAE in the variance task over randomly encoded inputs. Standard deviations computed over 5 random initialization runs are shown in parentheses. Best results (with statistical significance determined by a two-sample t -test at $p = 0.05$) are in bold.

Model	ρ	variance		range		maxmin	
		MAE ↓	time (s/epoch)	acc.↑	time (s/epoch)	acc.↑	time (s/epoch)
Deep Sets		70.3280(0.6886)	1.1869(0.0022)	0.0396(0.0026)	1.1687(0.0047)	0.0700(0.003)	1.1866(0.006)
JP 2-ary	Linear	3.5374(0.1926)	1.1758(0.0075)	0.0865(0.0045)	1.1564(0.0088)	0.0740(0.004)	1.1666(0.005)
Set Twister ($M=k=2$)		0.3697(0.0141)	1.7983(0.0070)	0.0904(0.0047)	1.7816(0.0251)	0.0790(0.002)	1.8200(0.013)

Table 10: Test accuracy and per-epoch training time in the maxmin task under different sequence lengths. Standard deviations computed over 5 runs are shown in parentheses. Best results (with significance determined by a two-sample t -test at $p = 0.05$) are in bold.

Model	$n_h=10$		$n_h=20$	
	acc.↑	time (s/epoch)	acc.↑	time (s/epoch)
DeepSets	0.615(0.009)	1.246(0.003)	0.538(0.012)	1.251(0.005)
Set Twister ($M=k=2$)	0.705(0.011)	1.746(0.017)	0.616(0.027)	1.768(0.015)
Set Twister ($M=3, k=2$)	0.702(0.007)	1.751(0.010)	0.632(0.012)	1.748(0.015)
Set Twister ($M=4, k=2$)	0.669(0.008)	1.759(0.013)	0.650(0.019)	1.847(0.007)

Table 8: Test MAE in the variance task and test accuracy in the range & maxmin task, using image inputs with linear ρ . Per-epoch training times are included for each task. Standard deviations computed over 5 random initializations are shown in parentheses. Best results (with statistical significance determined by a two-sample t -test at $p = 0.05$) are in bold.

Model	ρ	variance		range		maxmin	
		MAE ↓	time (s/epoch)	acc.↑	time (s/epoch)	acc.↑	time (s/epoch)
Deep Sets		1.582(0.017)	1.535(0.014)	0.350(0.005)	1.561(0.009)	0.345(0.002)	1.540(0.019)
JP 2-ary	Linear	0.974(0.032)	1.586(0.018)	0.475(0.009)	1.557(0.009)	0.354(0.007)	1.593(0.025)
Set Twister ($M=k=2$)		0.205(0.009)	2.085(0.007)	0.597(0.007)	2.120(0.020)	0.389(0.004)	2.124(0.033)

activation and output a scalar. This will help clarify empirically that Set Twister is more expressive than DeepSets (Zaheer et al. 2017) without the help of ρ . Comparing with 2-ary Janossy Pooling (Murphy et al. 2019a), we can further show its ability to capture 2-ary dependencies with $k = 2$.

The structure of the neural network and optimization routine remains the same for all different models in different tasks as shown in Table 1, Tables 2 and 7, except the change of ρ . We run all the models for 1,000 epochs. We omit the comparison with Set Transformer and Full Janossy Pooling

in this case since our main purpose here is to show the ability of Set Twister to capture higher order dependencies and being more expressive than DeepSets without the help of ρ .

We report the results for the image inputs in Table 8. From the table, we can see that Set Twister is always the best method for different tasks. In the 2-ary *variance task*, Set Twister achieves similar results with or without a nonlinear ρ compared with Table 1, demonstrating its ability to capture 2-ary dependencies. In the n_h -ary *range* and *maxmin* tasks, while Set Twister can not achieve comparable results to applying a nonlinear ρ , it does show significant improvements over 2-ary Janossy Pooling and DeepSets.

In Table 9, we can see the results over randomly encoded inputs. Same as the previous case, Set Twister outperforms in each task especially for *variance* task. Note that 2-ary Janossy Pooling is inherently able to capture 2-ary dependencies, although Set Twister does not perform well on the *range* and *maxmin* tasks, being comparable with 2-ary Janossy Pooling also shows its ability to capture 2-ary dependencies.

The effect of M and d_{rep} for Set Twister

We further study the effect of M for Set Twister. Note that we recommend to set $d_{\text{rep}} = d_{\text{DSrep}}/M$ to prevent the number of parameters exploding as we increase M . Here we also explore how setting d_{rep} being the same affects the performance when increasing M . We do this exploration on the hardest task we have, the *maxmin* task over random encoded integer inputs with vocabulary size 0 – 99.

Since DeepSets (Zaheer et al. 2017) corresponds to Set Twister with $M = k = 1$, we also include it in the comparison. First we use the same neural network structure and optimization routine as discussed in the paper and extend M to $M = 4$. In Table 7, there is a typo of $k = 3$ which should be $k = 2$, and we fix it in Table 10. From Table 10, we can see that when the sequence length is equal to 10, increasing M to $M = 4$ will significantly decrease the test accuracy. One possible reason is that the neural network structure for ϕ is $[60, 60]$ for DeepSets in this case, which means $d_{\text{rep}} = 60/4 = 15$ when we set $M = 4$. The small representation dimension thus restricts the capacity of the model. For sequence length equal to 20, increasing M shows improvement in performance with the current structure of ϕ being $[120, 120]$ for DeepSets. However, the performance improvement is not significant, showing that the simplest case $M = 2$ is enough to capture 2-ary dependencies.

Table 11: Test accuracy and per-epoch training time in the maxmin task under different sequence lengths when keeping d_{rep} the same. Standard deviations computed over 5 runs are shown in parentheses. Best results (with significance determined by a two-sample t -test at $p = 0.05$) are in bold.

Model	$n_h=10$		$n_h=20$	
	acc.↑	time (s/epoch)	acc.↑	time (s/epoch)
Set Twister ($M=k=2$)	0.694(0.008)	1.708(0.033)	0.454(0.022)	1.828(0.008)
Set Twister ($M=3, k=2$)	0.645(0.022)	1.795(0.012)	0.439(0.019)	1.800(0.016)
Set Twister ($M=4, k=2$)	0.617(0.012)	1.841(0.009)	0.437(0.026)	1.852(0.011)

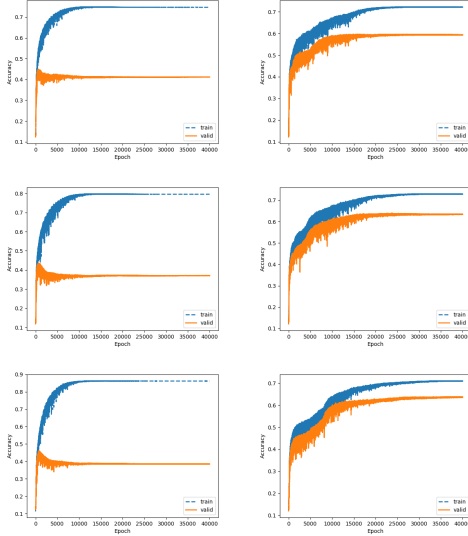


Figure 2: Training and validation accuracy for *maxmin* task over randomly encoded inputs with sequence length equal to 20. All the plots in the first column correspond to models with fixed d_{rep} , while the plots in the second column correspond to models with decreased d_{rep} . The first row represents models with $M = 2$, the second row represents models with $M = 3$, and the third row represents models with $M = 4$.

Next we set d_{rep} to be the same for any M . In our case $d_{\text{rep}} = d_{\text{DSrep}} = 120$. Now the first and second hidden layers of the neural network will have $[120M, 120M]$ hidden neurons. We use `relu` activation in this case since it gives better validation results, while keeping all the other optimization routines the same. We report the results in Table 11. From the table, we can see the accuracy decreases when increasing M . For sequence length equal to 20, the accuracy is significant worse than the previous cases in Table 10. We observe overfitting problems due to the increased number of parameters, which can be solved by more training data.

To visually understand the improvement in the model capacity, we plot the training accuracy and validation accuracy for different models in Figure 2. In the left column, we can see the improvement over training accuracy with the increase of M , meaning the model can fit the training data better with the increase of M when d_{rep} is fixed. In the right column we

do not see improvement of model capacities.

Comparison of `tanh` and `relu` activations

In most of our experiments, we use the `tanh` activation function for DeepSets and Set Twister as in Zaheer et al. (2017); Murphy et al. (2019a). Below, we also we report results using `relu` activations for DeepSets and Set Twister with all the other settings the same and show the empirical advantage of using `tanh` activation in Table 12, Tables 13 and 14.

Table 12: Test MAE in the variance task and test accuracy in the range & maxmin task, using image inputs for `relu` and `tanh` activations. Per-epoch training times are included for each task. Standard deviations computed over 5 random initializations are shown in parentheses. Best results (with statistical significance determined by a two-sample t -test at $p = 0.05$) are in bold.

Act.	Model	variance		range		maxmin	
		MAE↓	time (s/epoch)	acc.↑	time (s/epoch)	acc.↑	time (s/epoch)
<code>relu</code>	Set Twister ($M=k=2$)	0.643(0.038)	2.376(0.015)	0.760(0.025)	2.444(0.029)	0.332(0.005)	2.425(0.024)
	DeepSets	0.656(0.020)	1.798(0.005)	0.906(0.007)	1.782(0.026)	0.358(0.046)	1.727(0.043)
<code>tanh</code>	Set Twister ($M=k=2$)	0.200(0.007)	2.386(0.020)	0.931(0.002)	2.441(0.036)	0.931(0.003)	2.428(0.049)
	DeepSets	0.343(0.012)	1.804(0.015)	0.940(0.001)	1.842(0.012)	0.912(0.003)	1.839(0.012)

Table 13: Test accuracy and per-epoch training times in range and maxmin tasks and test MAE in the variance task over randomly encoded inputs for `relu` and `tanh` activations. Standard deviations computed over 5 random initialization runs are shown in parentheses. Best results (with statistical significance determined by a two-sample t -test at $p = 0.05$) are in bold.

Act.	Model	variance		range	
		MAE↓	time (s/epoch)	acc.↑	time (s/epoch)
<code>relu</code>	Set Twister ($M=k=2$)	0.181(0.020)	2.034(0.003)	0.808(0.032)	2.128(0.011)
	DeepSets	0.331(0.045)	1.522(0.010)	0.861(0.013)	1.506(0.008)
<code>tanh</code>	Set Twister ($M=k=2$)	0.333(0.008)	2.072(0.011)	0.944(0.004)	2.105(0.018)
	DeepSets	0.417(0.015)	1.501(0.016)	0.943(0.004)	1.504(0.006)

Table 14: Test accuracy and per-epoch training time in the maxmin task under different sequence lengths for `relu` and `tanh` activations. Standard deviations computed over 5 runs are shown in parentheses. Best results (with significance determined by a two-sample t -test at $p = 0.05$) are in bold.

Act.	Model	$n_h=10$		$n_h=20$	
		acc.↑	time (s/epoch)	acc.↑	time (s/epoch)
<code>relu</code>	Set Twister ($M=k=2$)	0.679(0.009)	1.770(0.013)	0.618(0.033)	1.773(0.012)
	Set Twister ($M=3, k=2$)	0.648(0.007)	1.814(0.015)	0.638(0.013)	1.678(0.012)
	Set Twister ($M=4, k=2$)	0.620(0.031)	1.824(0.008)	0.616(0.019)	1.767(0.012)
	DeepSets	0.596(0.006)	1.213(0.002)	0.517(0.016)	1.230(0.005)
<code>tanh</code>	Set Twister ($M=k=2$)	0.705(0.011)	1.746(0.017)	0.616(0.027)	1.768(0.015)
	Set Twister ($M=3, k=2$)	0.702(0.007)	1.751(0.010)	0.632(0.012)	1.748(0.015)
	Set Twister ($M=4, k=2$)	0.667(0.011)	1.759(0.013)	0.650(0.019)	1.847(0.007)
	DeepSets	0.615(0.009)	1.246(0.003)	0.538(0.012)	1.251(0.005)

From the tables, we can see using `tanh` activation gives significantly better results in most of the tasks, especially for the image inputs, which justifies our use of `tanh` activation.